Supplementary Information
Exploring separation techniques for the direct recycling of high voltage spinel LNMO scrap electrodes

Stiven Lopez Guzman[1,2], Marcus Fehse[1,*], Montse Galceran[1,*], Emanuele Gucciardi[1], Marta Cabello[1], Naiara Etxebarria[1], Silvia Martin[1], and Marine Reynaud[1,*]

[1]Center for Cooperative Research on Alternative Energies (CIC energiGUNE), Basque Research and Technology Alliance (BRTA), Alava Technology Park, Albert Einstein 48, 01510, Vitoria-Gasteiz, Spain.
[2]Chemical and Environmental Engineering Department, Faculty of Science and Technology, University of the Basque Country, UPV/EHU, B Sarriena, 48940 Leioa, Spain.
[*]Corresponding author: marcus.fehse@umontpellier.fr, mgalceran@cicenergigune.com, mreynaud@cicenergigune.com

December 3, 2024

1 Supplementary Figures

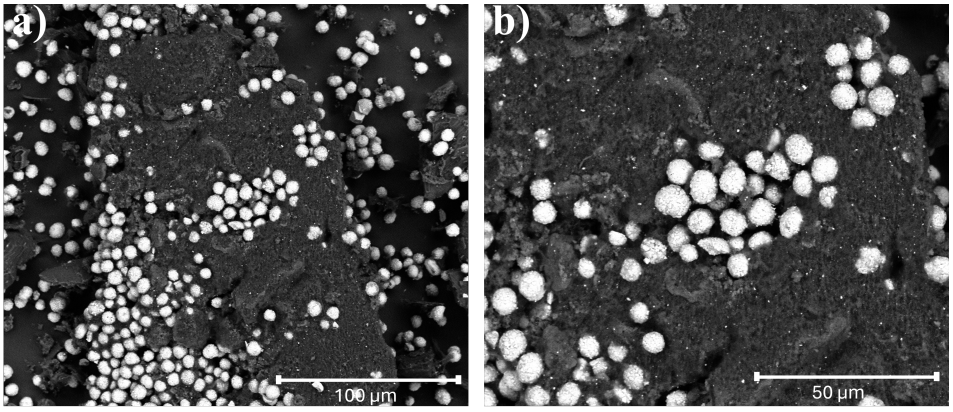

Figure 1: : SEM images of the chemical separation trial of LNMO-S samples using carbimide, with salient presence of a residue.

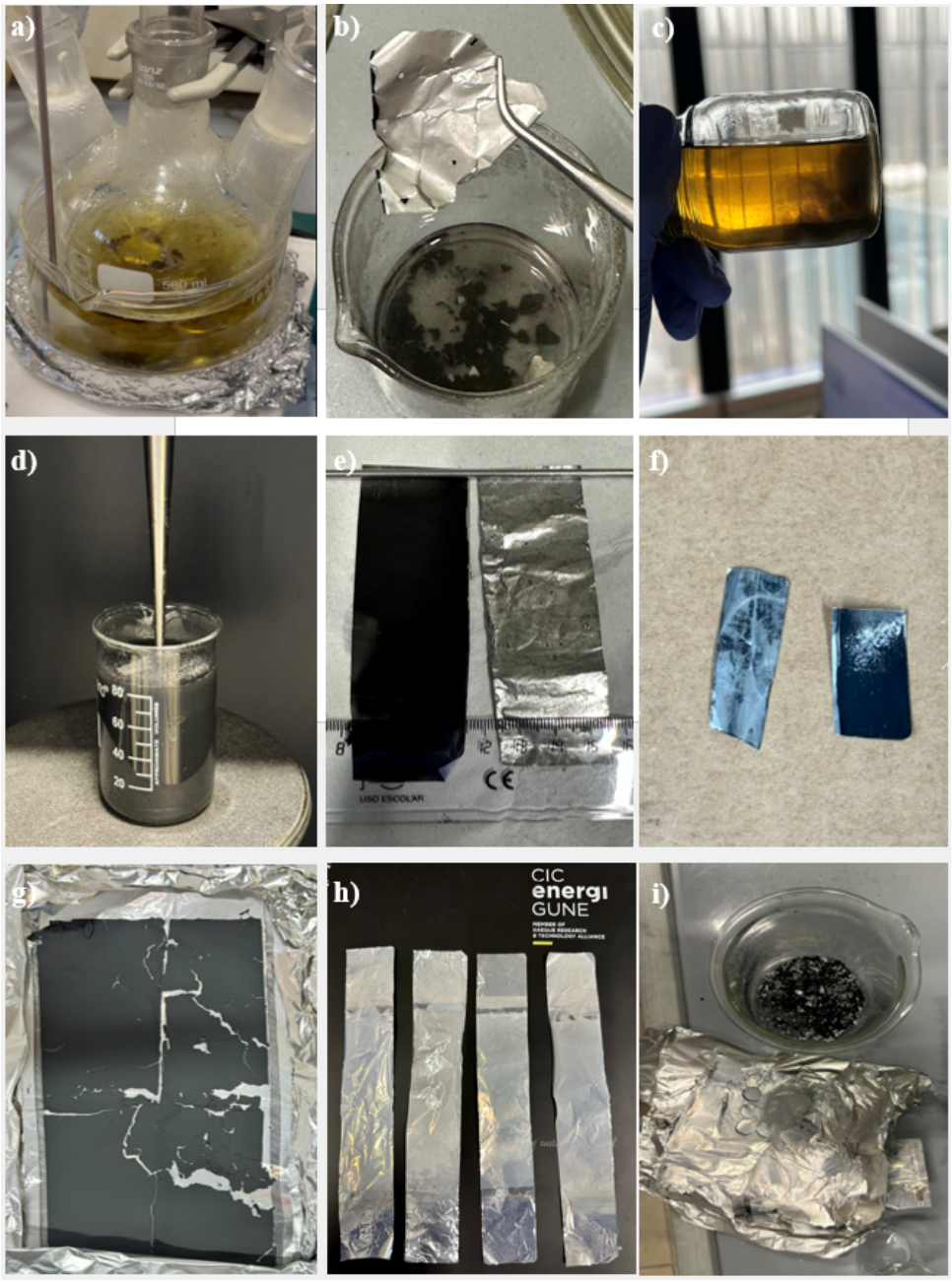

Figure 2: Diverse images of the separation procedure following the three separation methods. Chemical: a) The experimental setup where the active materials get delaminated some minutes after being introduced in the heated solution, b) completely delaminated Al current collector, and c) the residuals after the separation. Mechanical: d) experimental setup with the ultrasonic lance in water, e) before and after the delamination process, f) difference in in the delamination of the spherical (left) vs. the polygonal (right), which requires more energy to effectively separate the last. g) Resulting sample after the thermal delamination process, h) metallic current collectors after thermal delamination, free of residuals, i) degradation of Al when trying to employ higher temperatures during thermal separation

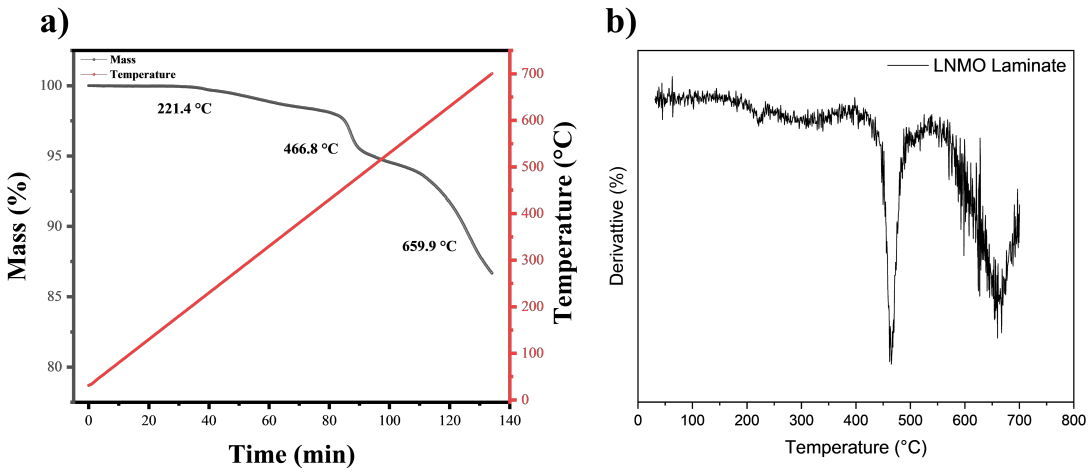

Figure 3: Thermogravimetric analysis (TGA) of a scrap aqueous LNMO electrode upon constant heating to 700^{o}C. b) corresponding first derivative of the TGA highlighting the temperature region of most pronounced mass loss .

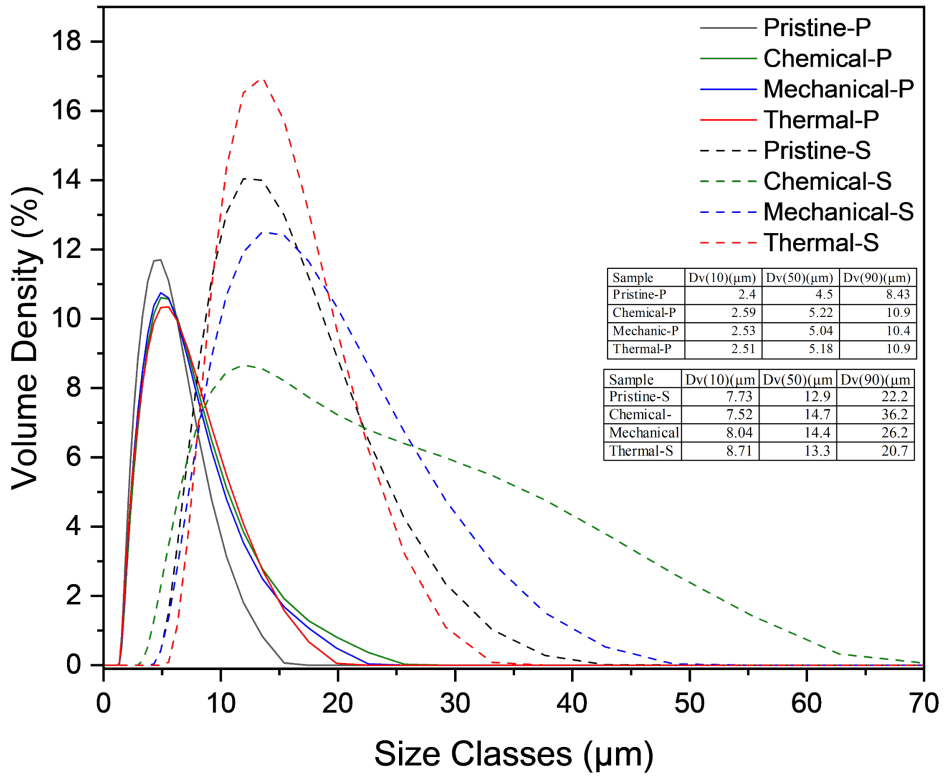

Sample	Dv(10)(μm)	Dv(50)(μm)	Dv(90)(μm)
Pristine-P	2.4	4.5	8.43
Chemical-P	2.59	5.22	10.9
Mechanic-P	2.53	5.04	10.4
Thermal-P	2.51	5.18	10.9

Sample	Dv(10)(μm	Dv(50)(μm	Dv(90)(μm
Pristine-S	7.73	12.9	22.2
Chemical-	7.52	14.7	36.2
Mechanical	8.04	14.4	26.2
Thermal-S	8.71	13.3	20.7

Figure 4: Particle size distribution of the spherical and polygonal samples.For LNMO-P (solid lines) and LNMO-S (dashed lines) of pristine powder(black), chemical (green), mechanical (blue), and thermal (red) recovered samples. The inset tables show the different Dv values for the measure particle size distribution

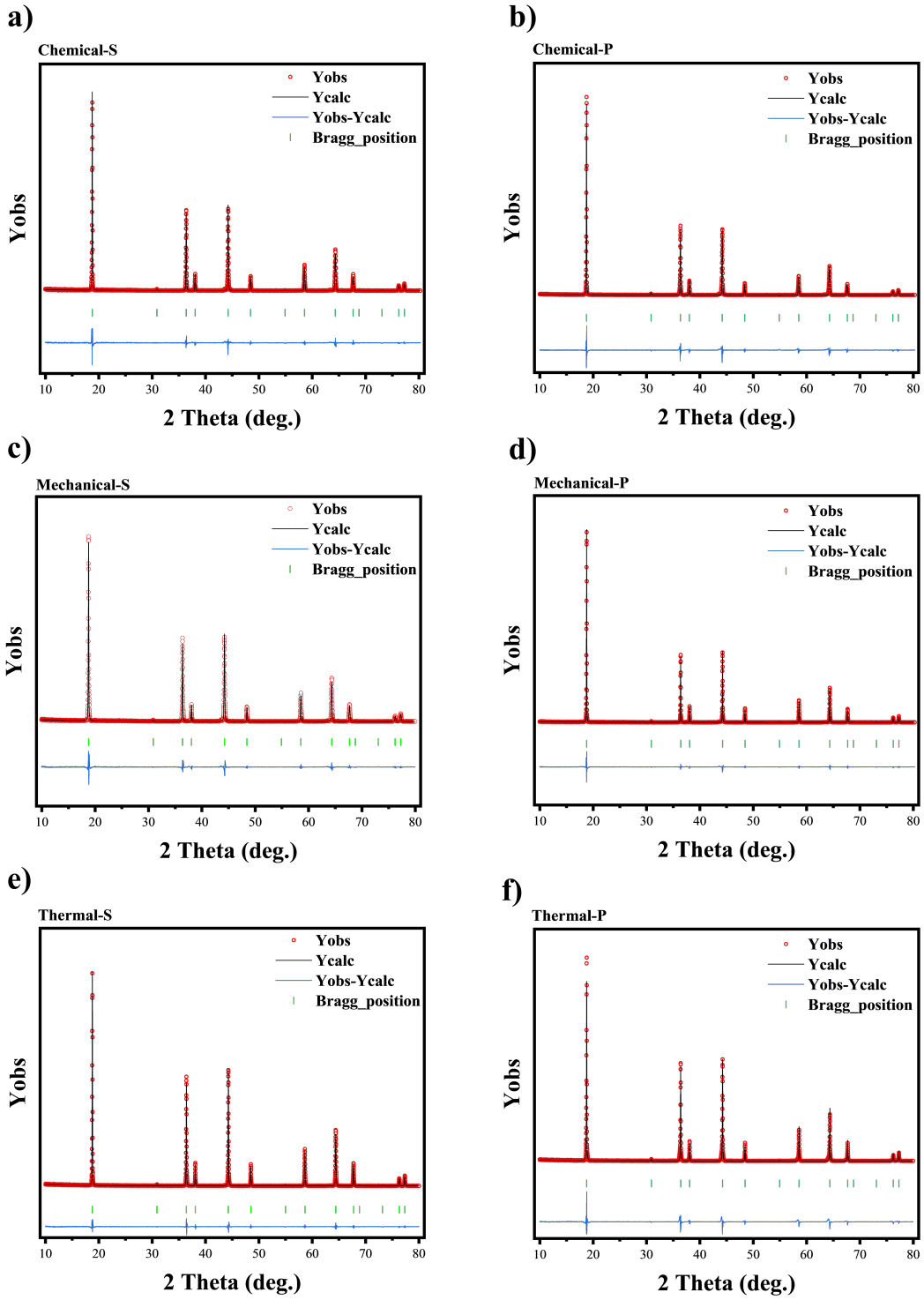

Figure 5: Rietveld refined X-ray diffraction patterns of the LNMO-S (left) and LNMO-P (right) chemical (top); mechanical (center) and thermal (bottom) recovered samples.

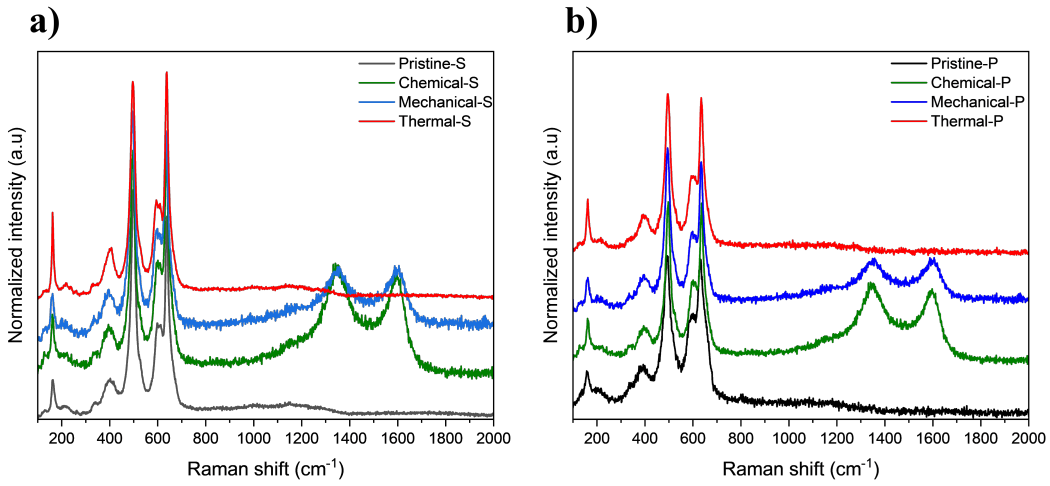

Figure 6: Extended Raman spectra showing the presence of the dual bands of carbon vibrational bonds for the Chemical (green) and Mechanical (blue) samples at 1357 and 1598 cm-1, in LNMO-S (a) and LNMO-P (b)

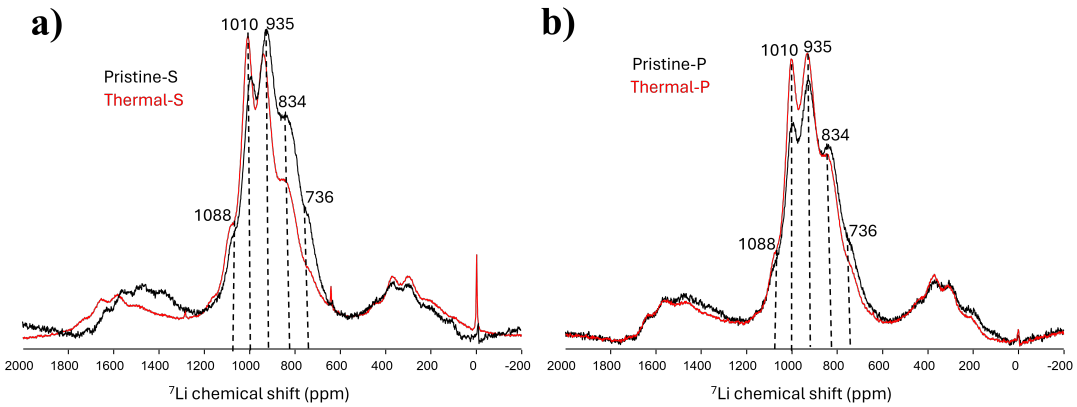

Figure 7: ^{7}Li ssNMR spectra of the a) LNMO-S (spherical) and b) LNMO-P (polygonal) samples against their corresponding thermal treated ones.

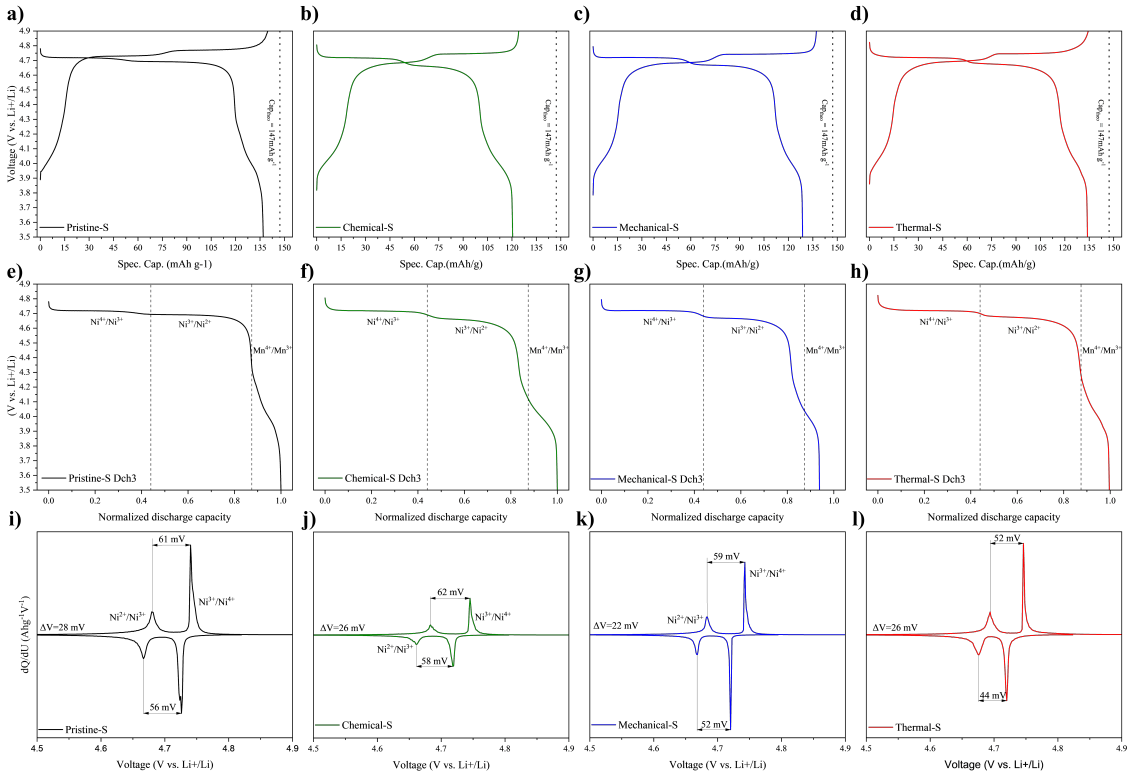

Figure 8: a-d) Charge and discharge profiles of the third cycle at 0.1 C of Pristine-S, chemical-S , mechanical-S and thermal-S, e-h) Normalized discharge profile of the third cycle to facilitate the comparison and identification of the characteristic oxidative reduction plateaus. i-l) dQ/dU plots of the corresponding charge discharge curves, the denoting the voltage gaps between the two nickel potentials, and the voltage polarization ΔV for the different spherical samples.

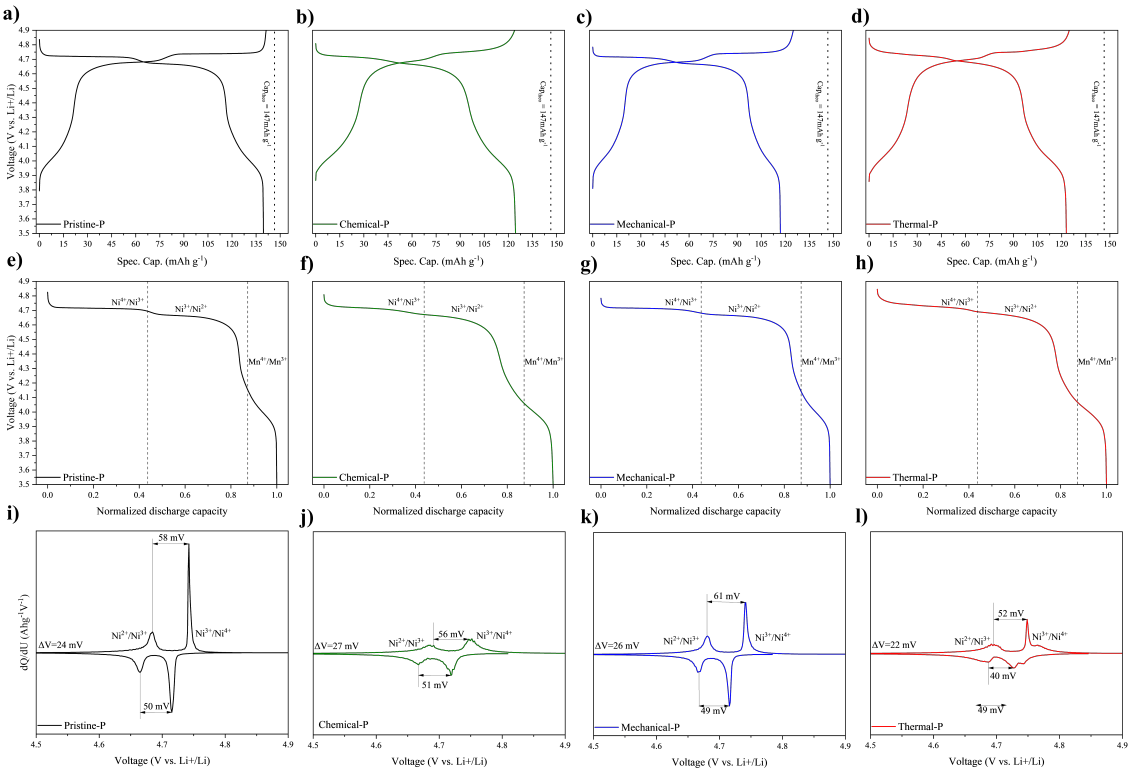

Figure 9: a-d) Charge and discharge profiles of the third cycle at 0.1 C of the pristine-P, chemical-P, mechanical-P and thermal-P e-h) Normalized discharge profile of the third cycle to facilitate the comparison of the high consistency in the prepared electrodes plus the identification of the characteristic oxidative reduction plateaus. i-l) dQ/dU plots, the denotation of the voltage gaps between the two nickel potentials, and the voltage polarization ΔV for the polygonal samples.

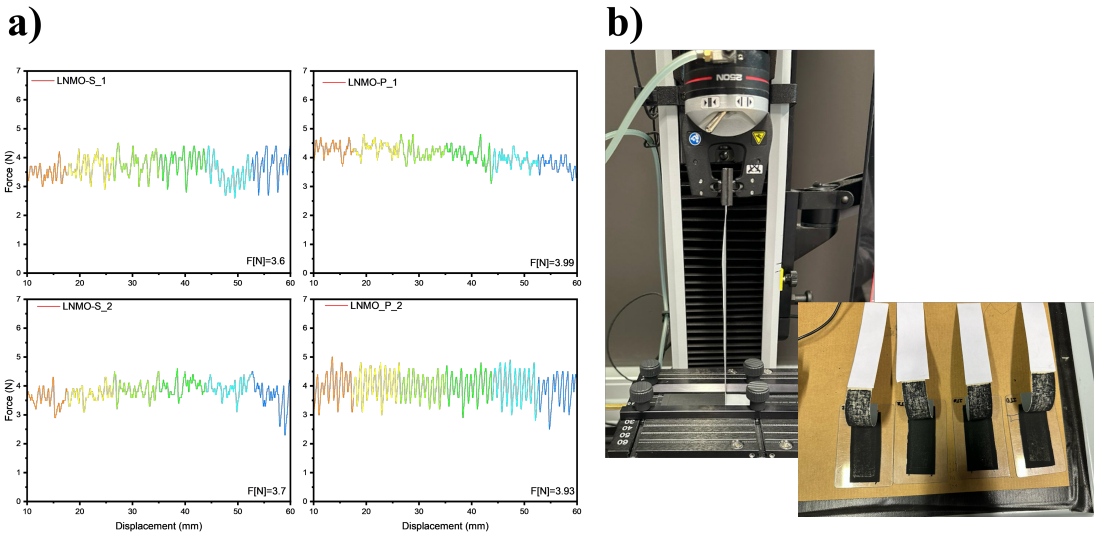

Figure 10: a) Force diagram showing the slight difference between the adhesion of the spherical and polygonal samples, b) some images of the experimental setup.

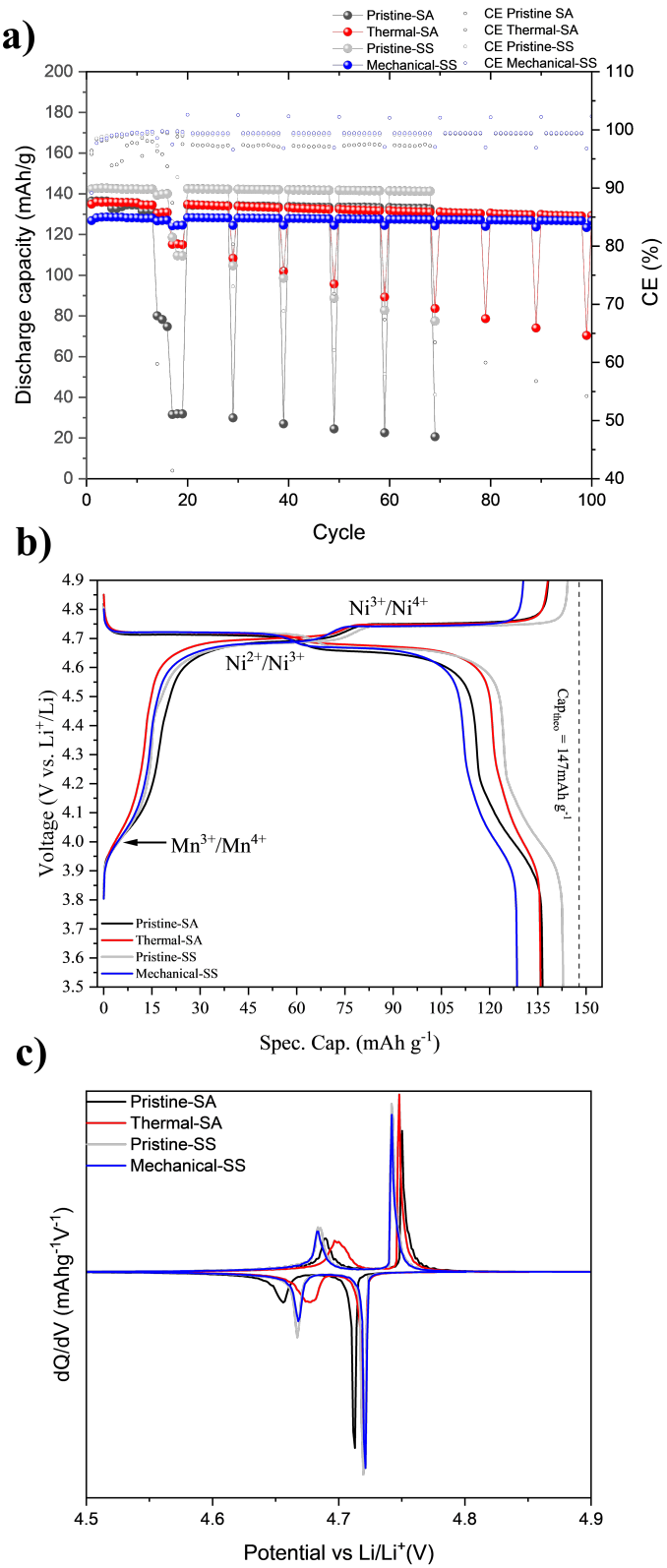

Figure 11: a) Cyclability, b) charge and discharge curves of the third cycle at 0.1 C, and c) the dQ/dV plot of the third cycle for both Spherical-SS and Spherical-SA samples.

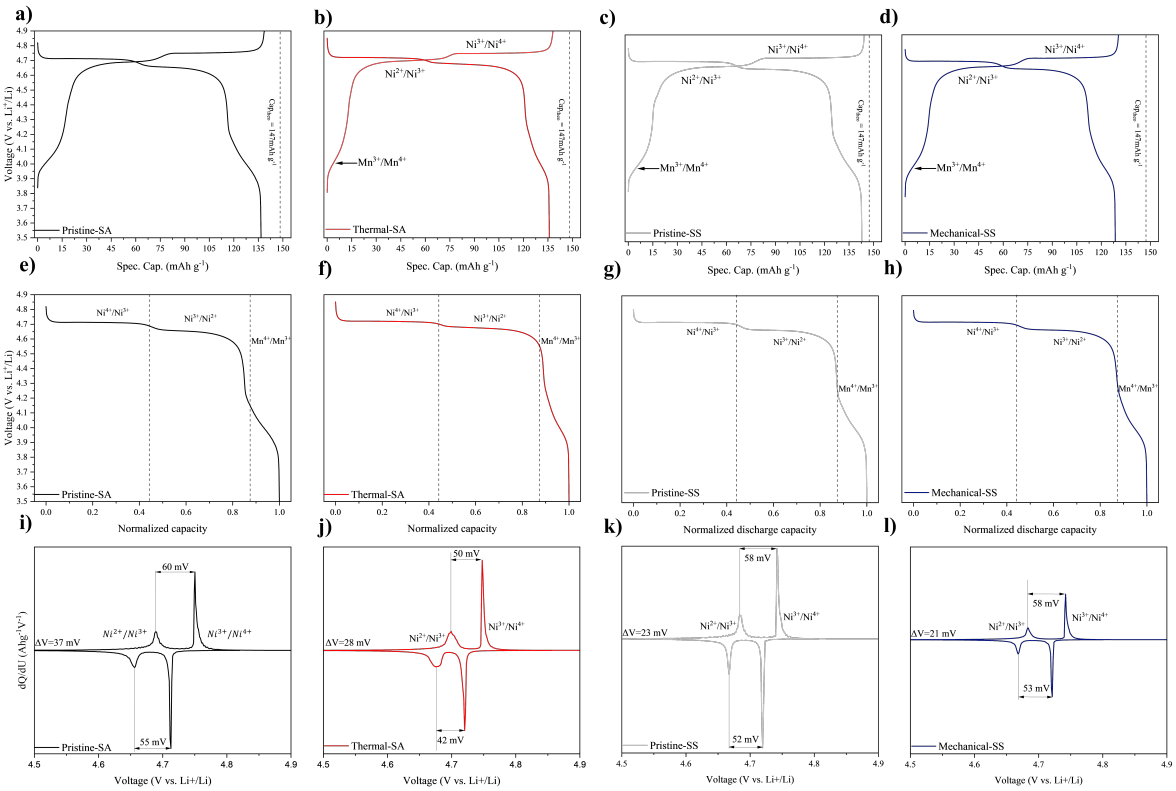

Figure 12: Charge and discharge profiles of the third cycle at 0.1 C of the a) Pristine-SA, b) Thermal-SA, c) Pristine-SS, and d) Mechanical-SS samples. Normalized discharge profile of the third cycle to facilitate their comparison and identify the characteristic oxidative reduction plateaus of the e) Pristine-SA, f) Thermal-SA, g) Pristine-SS, and h) Mechanical-SS samples. dQ/dU plots, the denotation of the voltage gaps between the two nickel potentials, and the voltage polarization ΔV for the different pristine and recycled spherical samples (i-l).

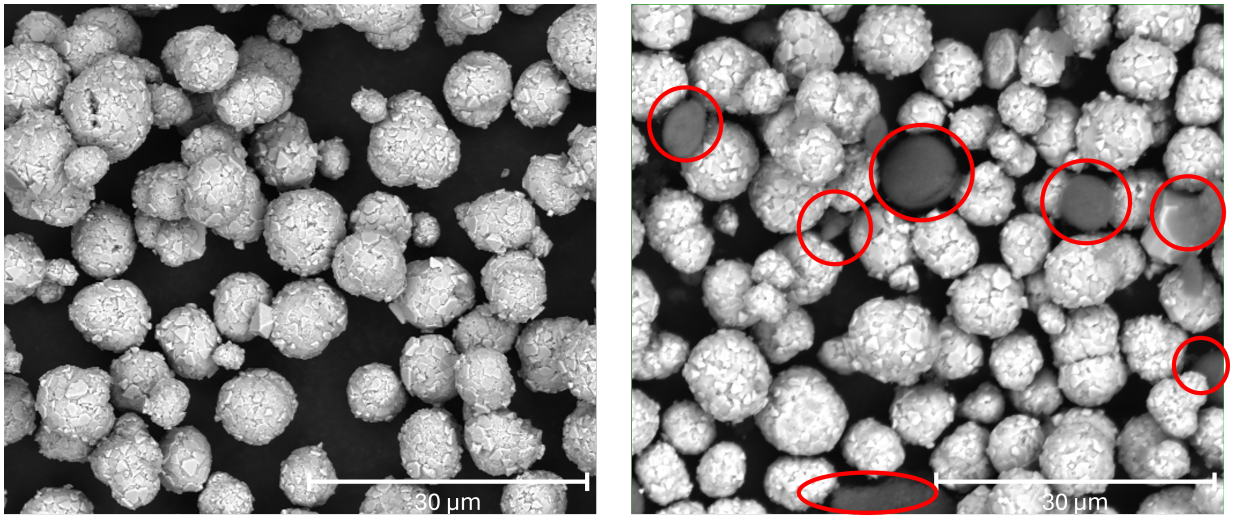

Figure 13: SEM micrographs providing a qualitative overview of the differences between the separation techniques. For the a) Thermal-SS, contaminants or residuals are absent, while for the b) Mechanical-SA, some carbon residues are present (indicated with the red circle) In both cased the LNMO samples conserve their specific spherical shape without any apparent distortion..

2 Supplementary Tables

Table 1: Cycling protocol of the LNMO cells.

Step number	**Current parameter**	**Number of cycles**
1	C/10 CCCV formation	2
	C/10 CCCV stabilization	2
2	C/5 CCCV symmetric	3
3	C/2 CCCV symmetric	3
4	1 C, Charge C/2	3
5	2 C, Charge C/2	3
6	3 C, Charge C/2	3
7	C/2	73
8	3 C, Charge C/2	8

Table 2: Molar ratio and standard deviation obtained from the ICP measurements.

Sample	**Li**	**Mn/Li**	**Ni/Li**	**Mn/Ni**	**Mn + Ni**	**Composition**
Pristine-S	1	1.53 ± 0.04	0.43 ± 0.01	3.51 ± 0.02	1.96 ± 0.05	$LiNi_{0.43}Mn_{1.53}O_4$
Chemical-S	1	1.42 ± 0.002	0.42 ± 0.004	3.37 ± 0.05	1.84 ± 0.01	$LiNi_{0.42}Mn_{1.42}O_4$
Mechanical-S	1	1.50 ± 0.002	0.42 ± 0.007	3.55 ± 0.005	1.93 ± 0.002	$LiNi_{0.42}Mn_{1.50}O_4$
Thermal-S	1	1.56 ± 0.001	0.46 ± 0.004	3.43 ± 0.03	2.02 ± 0.01	$LiNi_{0.46}Mn_{1.56}O_4$
Pristine-P	1	1.56 ± 0.03	0.42 ± 0.01	3.70 ± 0.07	1.98 ± 0.04	$LiNi_{0.42}Mn_{1.56}O_4$
Chemical-P	1	1.46 ± 0.05	0.41 ± 0.01	3.56 ± 0.01	1.87 ± 0.01	$LiNi_{0.41}Mn_{1.46}O_4$
Mechanical-P	1	1.51 ± 0.003	0.40 ± 0.004	3.76 ± 0.03	1.91 ± 0.01	$LiNi_{0.40}Mn_{1.51}O_4$
Thermal-P	1	1.58 ± 0.05	0.43 ± 0.01	3.73 ± 0.08	2.00 ± 0.05	$LiNi_{0.43}Mn_{1.58}O_4$

Table 3: Additional results obtained after the Le Bail refinement were obtained with the FullProf software.

Type	**Lattice constant (Å)**
Pristine-S	8.187(2)
Chemical-S	8.184(2)
Mechanical-S	8.183(2)
Thermal-S	8.176(1)
Pristine-P	8.186(1)
Chemical-P	8.183(2)
Mechanical-P	8.1816(1)
Thermal-P	8.1768(8)
Pristine-SS	8.180(2)
Thermal-SS	8.176(1)
Pristine-SA	8.185(2)
Mechanical-SA	8.183(9)

Table 4: Percentile recovery data of each separation technique after realizing four separation processes.

Route	**Chemical (%)**		**Mechanical (%)**		**Thermal (%)**	
Type	**Efficiency**	**Avg**	**Efficiency**	**Avg**	**Efficiency**	**Avg**
LNMO-S	88.51	86±2	87.36	90±3	93.32	91±4
	86.00		89.45		84.93	
	84.11		96.48		94.31	
	84.64		88.82		91.25	
LNMO-P	87.85	88±2	74.36	78±4	92.94	91±2
	90.33		83.90		92.77	
	88.71		75.20		87.27	
	85.88		80.36		92.69	

Table 5: Results corresponding to the elemental analysis for the separated samples.

Sample	**%C**	**%H**	**%N**	**%S**
Chemical-S	6.79 ± 0.01	0.11 ± 0.01	0.00	0.00
Chemical-P	2.89 ± 0.01	0.11 ± 0.01	0.00	0.00
Mechanical-S	4.94 ± 0.01	0.11 ± 0.01	0.00	0.00
Mechanical-P	1.73 ± 0.01	0.11 ± 0.01	0.00	0.00
Thermal-S	0.00	0.00	0.00	0.00
Thermal-M	0.00	0.00	0.00	0.00

Table 6: Summary of electrochemical results used to compare the effectiveness and performance of the recovered materials. The specific capacity is calculated as the average value of 3 cells after formation from cycle 7 after the initial formation process, the coulombic efficiency (CE) is for the first cycle, and the percentile capacity loss is calculated by comparing the first discharge with the last discharge value.

Type	**Specific capacity (mAh g^{-1})**	**First discharge capacity (mAh g^{-1})**	**CE (%)**	**Capacity loss final cycle (%)**
Pristine-S	140	137	95	7.2
Chemical-S	120	118	85	1.6
Mechanical-S	130	119	92	1.4
Thermal-S	133	133	90	3.1
Pristine-S	137	139	91	7.3
Chemical-S	122	122	92	0.7
Mechanical-S	120	118	93	0.5
Thermal-S	121	122	92	2.7
Pristine-SA	134	136	96	1.4
Thermal-SA	136	135	96	4.1
Pristine-SS	142	142	96	0.9
Mechanical-SS	128	127	89	1.2

Table 7: Voltage profile analysis and stoichiometry results.

Type	**$Mn^{3+/4+}$**	**$Ni^{2+/3+}$ + $Ni^{3+/4+}$**	**ν(Mn)**	**ν(Ni)**	**Composition**	**Composition ICP**
Pristine-S	14.2%	85.8%	1.57	0.43	$LiNi_{0.43}Mn_{1.57}O_4$	$LiNi_{0.43}Mn_{1.53}O_4$
Chemical-S	17.1%	82.9%	1.58	0.42	$LiNi_{0.42}Mn_{1.58}O_4$	$LiNi_{0.42}Mn_{1.42}O_4$
Mechanical-S	15.3%	84.7%	1.58	0.42	$LiNi_{0.42}Mn_{1.58}O_4$	$LiNi_{0.42}Mn_{1.50}O_4$
Thermal-S	14.4%	85.6%	1.57	0.43	$LiNi_{0.43}Mn_{1.57}O_4$	$LiNi_{0.46}Mn_{1.56}O_4$
Pristine-P	21.5%	78.5%	1.61	0.39	$LiNi_{0.39}Mn_{1.61}O_4$	$LiNi_{0.42}Mn_{1.56}O_4$
Chemical-P	25.6%	74.4%	1.63	0.37	$LiNi_{0.37}Mn_{1.63}O_4$	$LiNi_{0.41}Mn_{1.46}O_4$
Mechanical-P	19.3%	80.7%	1.60	0.40	$LiNi_{0.40}Mn_{1.60}O_4$	$LiNi_{0.40}Mn_{1.51}O_4$
Thermal-P	23.2%	76.8%	1.62	0.38	$LiNi_{0.38}Mn_{1.62}O_4$	$LiNi_{0.42}Mn_{1.58}O_4$
Pristine-SA	17.6%	82.4%	1.59	0.41	$LiNi_{0.41}Mn_{1.59}O_4$	
Thermal-SA	13.0%	87.0%	1.57	0.43	$LiNi_{0.43}Mn_{1.57}O_4$	
Pristine-SS	15.3%	84.7%	1.58	0.42	$LiNi_{0.43}Mn_{1.57}O_4$	
Mechanical-SS	14.7%	85.3%	1.57	0.43	$LiNi_{0.43}Mn_{1.57}O_4$	